Journal of Power Sources 244 (2013) 435–441

Contents lists available at SciVerse ScienceDirect

Journal of Power Sources

journal homepage: www.elsevier.com/locate/jpowsour

Facile approach to synthesize CuO/reduced graphene oxide nanocomposite as anode materials for lithium-ion battery

Alok Kumar Rai, Ly Tuan Anh, Jihyeon Gim, Vinod Mathew, Jungwon Kang, Baboo Joseph Paul, Nitish Kumar Singh, Jinju Song, Jaekook Kim*

Department of Materials Science and Engineering, Chonnam National University, 300 Yongbong-dong, Bukgu, Gwangju 500-757, Republic of Korea

HIGHLIGHTS

- Copper oxide (CuO) nanoparticles were synthesized by low cost facile microwave-assisted method.
- Nanocomposite was synthesized by short-time spex-milling of CuO and 10 wt% graphene nanosheets.
- Nanocomposite anode exhibited high rate capability and excellent cyclic stability.
- Excellent performance can be attributed to synergistic effect between CuO and reduced graphene.
- Simple, low cost and short-time synthesis is attractive for practical application in large scale.

ARTICLE INFO

Article history:
Received 5 October 2012
Received in revised form
26 November 2012
Accepted 27 November 2012
Available online 1 December 2012

Keywords:
Copper oxide
Graphene
Spex mill
Anode
Lithium ion battery

ABSTRACT

An efficient synthesis is used for the first time to prepare CuO/reduced graphene oxide nanocomposite anode materials for lithium ion batteries. Initially, copper oxide (CuO) nanoparticles are synthesized via a simple, facile and inexpensive microwave-assisted method within short reaction times (<20 min) and subsequent heat treatment at 500 °C for 5 h. The obtained pure CuO nanoparticles are mixed with 10 wt% of graphene nanosheets by the use of spex mill for 1 min. By short-time spex-milling, a unique CuO/reduced graphene oxide nanocomposite is obtained with a microstructure of multi-scale CuO nanoparticles homogeneously dispersed in a graphene matrix. The synthesized samples are characterized using X-ray diffraction and field-emission transmission electron microscopy studies. The spex-milled nanocomposite anode exhibits better electrochemical performance with higher reversible capacity and excellent cyclability in comparison with pure CuO nanoparticles. The initial discharge capacity of the pure CuO nanoparticles and their nanocomposite are 785.2 mAh g^{-1} and 1043.3 mAh g^{-1} with reversible capacity retention of 392.1 mAh g^{-1} and 516.4 mAh g^{-1} after 45 cycles respectively. The excellent electrochemical performance of CuO/reduced graphene oxide nanocomposite can be attributed to their unique structures, which intimately combine the conductive graphene nanosheets network with uniformly dispersed CuO nanoparticles.

1. Introduction

Rechargeable lithium-ion batteries have attracted great attention for their utilization in portable electronic devices, electric vehicles (EV) and high power hybrid electric vehicles (HEV) [1–3]. In order to develop better high power electrical devices, high capacity, long cycle life and good rate capability are the essential requirements to develop electrode materials for new-generation high-power lithium-ion batteries. But the intrinsic properties of the electrodes limit the lithium insertion rate, charge–discharge current and the energy density. To avoid the rate issues, several alternative approaches have been pursued, in which either the existing electrodes were replaced by better materials or modified to nanostructured form. In this context, nanostructured electrode materials are seemingly the most promising candidate to provide multiple advantages such as a short path distance for Li ions and electron transport, a higher contact area with electrolyte and better accommodation of the strain caused by lithiation or delithiation [4]. The conventional graphite anode materials have a low theoretical capacity (372 mAh g^{-1}), which limits its further application in electrical devices requiring a higher energy density [5]. Despite many potential high-capacity anode materials, such as transition

* Corresponding author. Tel.: +82 62 530 1703; fax: +82 62 530 1699.
E-mail address: jaekook@chonnam.ac.kr (J. Kim).

0378-7753/$ – see front matter © 2012 Elsevier B.V. All rights reserved.
http://dx.doi.org/10.1016/j.jpowsour.2012.11.112

metal oxides (CoO, NiO, CuO, Fe_2O_3, $Fe_{1-x}O$ etc.), lithium alloy (Li–M, M = Sn, Si, Sb, Al, etc.) and tin based (Co–Sn–C) anodes have been suggested to substitute for graphite anodes [6–11], the improvement of cycle life, reversible capacity, and high-rate performance of the electrode materials is still ongoing. Among the most attractive candidates, transition-metal oxides could be a new class of promising anode materials for lithium-ion batteries. The transition metal oxides react reversibly with lithium in lithium cells below 1.5 V and demonstrate large theoretical capacity (about 700 mAh g^{-1}) and long cycle life [12].

Cupric oxide (CuO), well-known material of p-type semiconductor, has been employed for gas-sensors [13], solar energy conversion [14], and lithium-ion battery anode materials [15,16], because of their low band-gap energy and high catalytic activity, as well as their nontoxic nature and affordable price. However, CuO anode suffered from rapid capacity fading due to large volume expansion/contraction during cycling process and severe particle aggregation associated with the Li^+ insertion and extraction process which lead to the electrode pulverization and loss of interparticle contact [12,17–20]. To avoid this problem, carbonaceous materials with high flexibility and electrical conductivity have been widely used as matrices for CuO anodes to improve their lithium-ion storage properties [9,16,21].

Graphene is an excellent substrate to load nanomaterials for energy applications due to its large surface area, excellent conductivity, mechanical strength, chemical stability and light weight [22–24]. In addition, graphene produced by the chemical reduction of graphene oxide has abundant functional groups on the surface, such as –COOH and –OH, and thus may provide a better connection with other materials to form a homogeneous composite or hybrid by interfacial interaction with some active particles during preparation [25,26]. Recently, some graphene based nanocomposite electrode materials such as Co_3O_4/graphene, Fe_3O_4/graphene, Sn@C/graphene and $Li_4Ti_5O_{12}$/graphene have been reported to enhance the storage capacity and cyclic stability [27–32]. In these composites, graphene nanosheets not only decrease the contact resistance of active particles and improve electrical conductivity of the electrode but also prevent the aggregation of nanoparticles during cycling.

In this paper, first we have successfully synthesized pure CuO nanoparticles via a simple and inexpensive microwave-assisted synthesis method under short time duration. For the synthesis of CuO/reduced graphene oxide nanocomposite, the obtained pure CuO nanoparticles are mixed with 10 wt% of graphene nanosheets by the use of spex mill for 1 min. The obtained final products are characterized using powder X-ray diffraction pattern and field-emission transmission electron microscopy. In addition, the electrochemical performance of the as-obtained CuO/reduced graphene oxide nanocomposite as an anode material for lithium ion battery was investigated and compared with pure CuO nanoparticles electrode. Graphene is chosen as a conductive additive to form a well connected conductive network and reduce the difference between charge and discharge potentials plateau at all rates. It is found that the CuO/reduced graphene oxide nanocomposite exhibits significantly improved rate capability and excellent cycling performances in comparison to pure CuO nanoparticles.

2. Experimental

2.1. Preparation of graphene oxide and graphene nanosheets

Initially, graphene oxide was prepared by the oxidation of graphite (Daejung Chemical) using a modified Hummers method [33]. Further, the graphene nanosheets were developed by a simple polyol-based approach involving the reduction of graphene oxide. Detailed preparation procedure for the graphene nanosheets can be found in our previous paper [34].

2.2. Materials synthesis

In a typical synthesis, analytical grade copper (II) acetate ($Cu(CH_3COO)_2 \cdot H_2O$) (98+%, Aldrich) was used as the precursor. In a typical synthesis, 0.01 mol of copper acetate was dissolved in 50 ml of deionized water (DI) with magnetic stirring at room temperature to form a homogeneous solution, and then ammonia solution (10 ml, Daejung 25%) was added to the above solution. After being stirred for 3 h, the resulting mixture was transferred to a conventional microwave oven (MM-M 301, LG-Korea) with the specification of 1000 W at 2450 MHz. And then, the obtained solution was heated around 140–150 °C for 10 min by microwave irradiation. After the reaction, the product was cooled to room temperature. The resultant as-prepared dried mixtures were ground to fine powders before heating at 500 °C for 5 h in an air atmosphere. The obtained powder after heating at 500 °C is designated here as pure CuO nanoparticles.

Nanocomposite of pure CuO nanoparticles and reduced graphene nanosheets was prepared by milling under very short time duration. A schematic sketch about the formation of nanocomposite shown in Scheme 1 describes the experimental procedure. Spex mill (Spex MM 400, Retsch) with 10 ml hardened steel bowl filled with 2 hardened steel balls in the diameter of 10 mm was used for milling. The obtained above pure CuO nanoparticles were mixed with 10 wt% of reduced graphene nanosheets for 1 min. The mixer/mill was a vibration type and the milling cylinder vibrated with high amplitude and frequency of 50/60 Hz. The resulted product is designated here as CuO/reduced graphene oxide nanocomposite.

2.3. Materials characterization

The X-ray diffraction (XRD) patterns were obtained by a Shimadzu X-ray diffractometer with Cu Kα radiation (λ = 1.5406 Å).

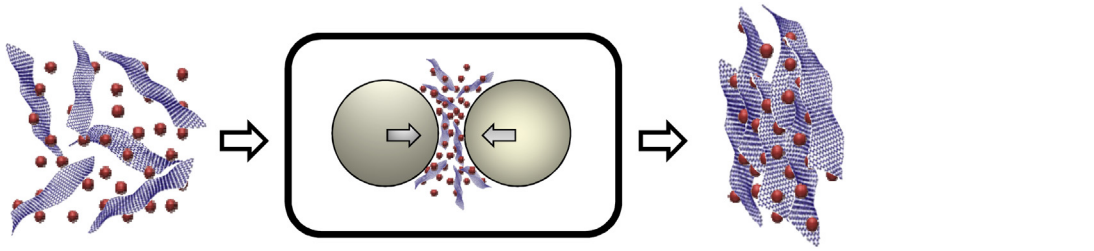

Scheme 1. Schematic illustration of the preparation of CuO/reduced graphene oxide nanocomposite.

The morphology of the final products was characterized by field-emission transmission electron microscopy (FE-TEM) and high-resolution transmission electron microscopy (HR-TEM) by a FEI Tecnai F20 with an accelerating voltage of 200 kV. For the FE-TEM images, these samples were ultrasonically dispersed in ethanol and a few drops were coated on copper grids and the solvent was subsequently allowed to evaporate in air at room temperature. Surface area can be determined based on the nitrogen adsorption and desorption isotherms using Brunauer–Emmett–Teller (BET, Micromeritics ASAP2010 Instrument Co., Norcross, GA, USA).

2.4. Electrochemical measurements

Electrochemical experiments were carried out using 2032 coin-type cells assembled in an argon-filled glovebox. The working electrodes were prepared by mixing the active material (pure CuO nanoparticles and their nanocomposite) with super-P and poly vinylidene difluoride (PVDF) at a weight ratio of 80:10:10 in *N*-methyl-2-pyrrolidone (NMP) to form a slurry. Then, the resultant slurry was uniformly pasted on Cu-foil with a blade, dried at 120 °C in a vacuum oven and pressed between stainless steel twin rollers. Afterward, the foil was punched into circular discs, and coin cells were assembled with lithium metal as the counter electrode and a Celgard 2400 membrane together with glass fiber as a separator. The cells were kept in a glovebox for 12 h before electrochemical measurements. The electrolyte used was 1 M $LiPF_6$ dissolved in a mixture of ethylene carbonate (EC) and dimethylcarbonate (DMC) (1:1 in volume ratio). The discharge–charge measurements (BTS-2004H, Nagano, Japan) were performed over the potential range of 0.01–3.0 V vs. Li^+/Li at different current densities. Furthermore, when the upper cut-off voltage was reduced to 2.0 V, the material delivers a considerable loss in the capacity value. However, in order to understand the characteristic charging curve of CuO around 2.5 V, the discharge/charge measurements in the present work were performed in the voltage region of 0–3.0 V. Electrochemical impedance spectroscopy (EIS) measurements of the electrode were carried out on an AUTOLAB potentiostat (PGSTAT302N). Before the measurements, the electrode was cycled for 3 cycles and then measured in the frequency range from 0.01 Hz to 1.0 MHz. A small ac signal of 5 mV in amplitude was used as the perturbation of the system throughout the tests. EIS was used to measure the electronic conductivities of the assembled cell using lithium foil acting as both the counter and reference electrodes.

3. Results and discussion

3.1. Crystal structure and morphology

The purities of the prepared CuO nanoparticles and their nanocomposites were confirmed by XRD. Fig. 1(a and b) shows the XRD patterns of the obtained pure CuO nanoparticles and CuO/reduced graphene oxide nanocomposite, respectively. Both of the patterns can be indexed as a monoclinic symmetry (JCPDS Card No. 05-0661) with *C*2/*c* space group. No impurities could be detected in the XRD patterns. The (002) peak of graphene nanosheets is shadowed by the high intensities of Al holder and CuO peaks in the nanocomposites sample.

FE-TEM micrographs of pure CuO nanoparticles and CuO/reduced graphene oxide nanocomposite are shown in Fig. 2. The FE-TEM picture shown in Fig. 2, provides information on the size and morphology of the CuO nanoparticles and their state of agglomeration. As shown in Fig. 2(a), agglomerated nanostructures of the pure CuO nanoparticles can be observed in FE-TEM image and the particle size is in the range of 60–65 nm. A few smaller nanoparticles aggregate into secondary particles probably due to

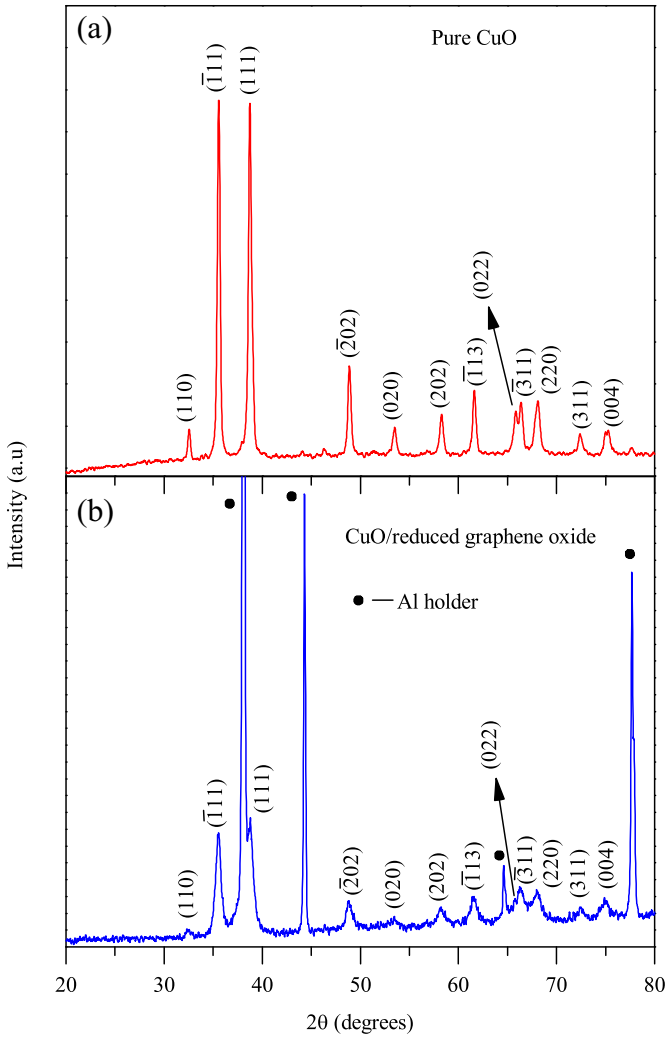

Fig. 1. X-ray diffraction patterns of (a) pure CuO nanoparticles and (b) CuO/reduced graphene oxide nanocomposite.

their extremely small dimensions and high surface energies. The resulting large particles would lead to the poor rate performance as an anode material due to the long diffusion path for electron and Li-ion transport during the Li-ion insertion/extraction process. Fig. 2(b) represents the HR-TEM image of the sample which indicates the high crystalline nature of the sample. The interplanar spacing '*d*' (distance between two successive lines) measured from the fringe pattern is 2.3 Å, which corresponds to the (200) plane, as observed from the XRD results in Fig. 1. Fig. 2(c) shows the FE-TEM image of CuO/reduced graphene oxide nanocomposite prepared by the facile spex-mill synthesis approach. Obviously, the deposition of CuO nanoparticles onto the surfaces of reduced graphene nanosheets is homogeneous. It should be pointed out that the random hybridization between CuO nanoparticles and reduced graphene nanosheets can form highly conducting two dimensional (2D) graphene electronic conductive network of the CuO/reduced graphene oxide nanocomposite. Particle sizes are in the range of 40–65 nm and slightly smaller than that observed in pure CuO nanoparticles. Another phenomenon is that, even after a long time of sonication during the preparation of the TEM specimen, the CuO nanoparticles were still strongly anchored on the surface of reduced graphene nanosheets with a high density, implying the strong interaction between CuO nanoparticles and reduced graphene nanosheets. We believe that such interaction combined with

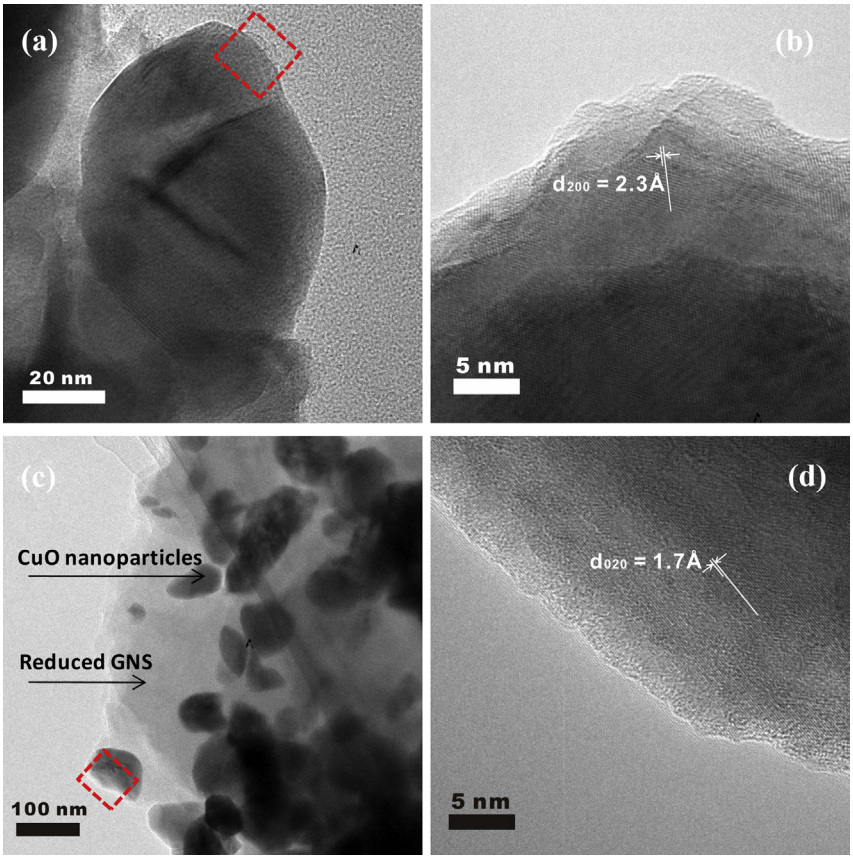

Fig. 2. FE-TEM and HR-TEM images of pure CuO nanoparticles (a and b) and CuO/reduced graphene oxide nanocomposite (c and d) respectively.

good mechanical flexibility of reduced graphene nanosheets prevents the agglomeration of nanoparticles to large particles, in the presence of reduced graphene nanosheets. In addition, the strong anchoring of small CuO nanoparticles on reduced graphene nanosheets enables fast electron transport through the underlying graphene layers to nanoparticles to improve the electrochemical performance. Fig. 2(d) is HR-TEM image of CuO/reduced graphene oxide nanocomposite, showing the well crystalline nature of CuO nanostructures. The lattice fringe spacing of 1.7 Å corresponds to the (020) plane of CuO crystal.

N_2 adsorption/desorption isotherms were employed to investigate the surface area of CuO/reduced graphene oxide nanocomposite and the pure CuO nanoparticles. It is desirable for anode materials to have higher surface areas that are able to increase the electrode and electrolyte contact area and favors fast Li ion insertion/extraction in the sample. However, the BET specific surface area of pure CuO nanoparticles and CuO/reduced graphene oxide nanocomposite are 2.0 $m^2\ g^{-1}$ and 37.7 $m^2\ g^{-1}$, respectively. Obviously, the BET specific surface area of nanocomposite is much higher than that of pure CuO nanoparticles, which is due to the good quality of reduced graphene nanosheets with high surface area. These factors may lead to the increased electrochemical reactivity in the nanocomposite [35].

3.2. Electrochemical performance

Pure CuO nanoparticles and their nanocomposite electrodes were examined with Li-ion insertion and extraction to demonstrate their electrochemical performance in energy storage. The assembled cell was cycled between 0.01 and 3.0 V at room temperature with a current density of 0.1 mA cm^{-2}. Fig. 3(a and b) shows the discharge/charge voltage profiles of the pure CuO nanoparticles and their nanocomposite electrodes, respectively, up to the 5th cycle. It can be clearly observed that the initial discharge/charge voltage profiles as well as stabilized ones for the pure CuO and CuO/reduced graphene oxide electrodes are very similar, implying that the introduction of reduced graphene nanosheets does not change the nature of CuO. After the 1st cycle, the curves of each cycle are similar in shape, indicating that the electrode reactions become more reversible. The slopes in each discharge/charge curve are in the same position and similar to those of CuO materials reported in the literatures [16,36]. The initial discharge capacity is around 785.2 mAh g^{-1} and 1043.3 mAh g^{-1} for the pure CuO nanoparticles and their nanocomposite electrodes (determined on basis of the total mass of CuO and reduced graphene oxide) respectively, which are much higher than the theoretical specific capacity of pure CuO (670 mAh g^{-1} based on the electrode reaction $CuO + 2Li^+ + 2e^- \leftrightarrow Cu + Li_2O$). The extra capacity compared with the theoretical capacities is usually ascribed to the formation of solid electrolyte interface (SEI) layer during the initial discharge process, some of the Cu (0) cannot be re-oxidized back to Cu (II), the reduction of the adsorbed impurities on active material surfaces and the initial formation of lithium oxide as well as possibly interfacial lithium storage [37]. The SEI is a gel-like organic layer, and it consist of ethylene-oxide-based oligomers, LiF, Li_2CO_3, and lithium alkyl carbonate [38]. More importantly, the voltage profile of the nanocomposite electrode displays smaller polarization ($V_{ch} - V_{dis}$) than that of the pure CuO nanoparticles is due to the electronically conducting graphene nanosheets that provides better intimate connectivity between the CuO nanoparticles.

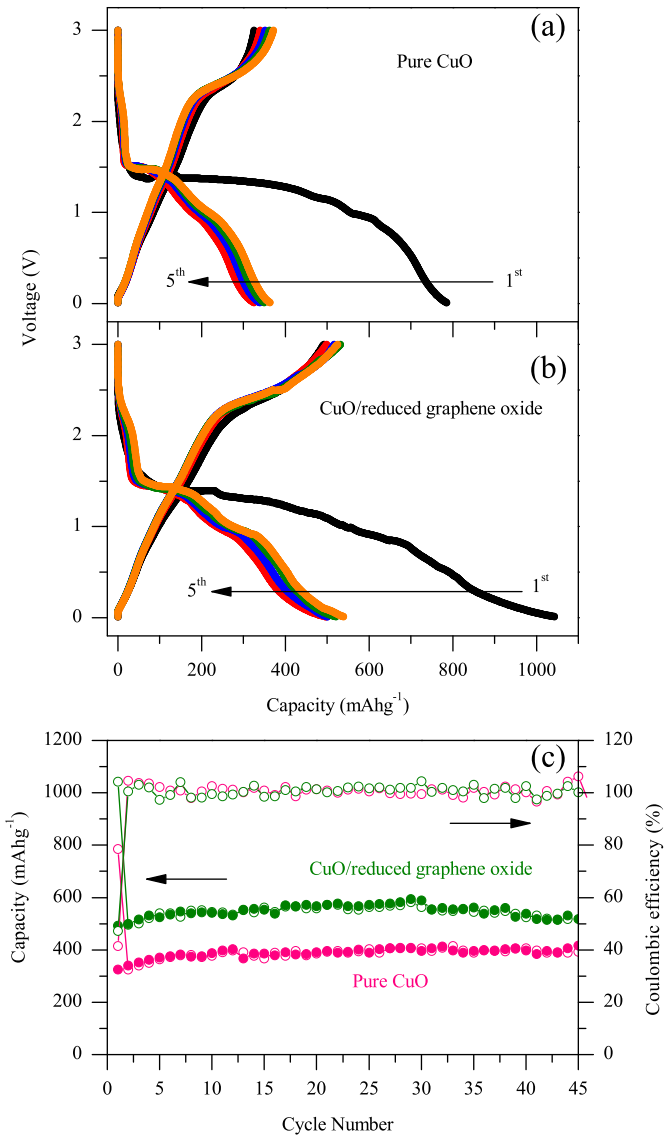

Fig. 3. First five discharge/charge curves of (a) pure CuO nanoparticles and (b) CuO/reduced graphene oxide nanocomposite and (c) their cycling performance between 0.01 and 3.0 V (vs Li^+/Li) at a current density of 0.1 mA cm^{-2}.

Moreover, the CuO/reduced graphene oxide nanocomposite shows more extra reversible capacity compared to that of pure CuO nanoparticles electrode, which can be attributed to large electrochemical active surface-area of well-dispersed reduced graphene nanosheets, reduced resistance, polarization of the electrode and more grain boundary areas of the CuO nanoparticles in the composite. On the other hand, the nanocomposite electrode has higher initial coulombic efficiency than the pure CuO nanoparticles electrode such as 47.2% and 42% respectively. It is also reasonable to suggest that the introducing of reduced graphene nanosheets shows a strong synergetic effect in the composite for improving the reversible capacity. Interestingly, both the CuO and their nanocomposite electrode shows the negligible decay of charge/discharge capacity during consecutive cycling than the reported capacity fading observed for pure CuO electrode [14,39].

Another advantage of the CuO/reduced graphene oxide nanocomposite is significantly improved cycling performance compared with pure CuO nanoparticles electrode. Fig. 3 (c) shows the cycling behavior of the pure CuO nanoparticles and their nanocomposite electrodes at a constant current density of 0.1 mA cm^{-2}. It can be clearly observed that the capacity plots of the discharge and charge cycles of both the pure CuO nanoparticles and their nanocomposite overlap with each other from the 2nd to the 45th cycles. This trend indicates that the columbic efficiencies of almost 100% will be achieved during extensive cycling. On the other hand, both pure CuO nanoparticles and their nanocomposite electrodes exhibit second reversible capacity are ca. 325.6 mAh g^{-1} and 496.5 mAh g^{-1} respectively. Moreover, in both the case of pure CuO nanoparticles and their nanocomposite electrode, the capacity does not fade but increases gradually to ca. 392.1 mAh g^{-1} and 516.4 mAh g^{-1} respectively over 45 cycles, which are equivalent to ca. 80% and 90% of the second reversible capacity, demonstrating excellent capacity retention of the electrodes. The coulombic efficiency is about 42–47% in the first cycle, while it increases to about 100% in the second cycle and maintains at this value for the rest cycles. The phenomenon for capacity increase has also been observed on carbon/iron oxide and Cu nanowires/Fe_3O_4 anode materials [40,41], and was attributed to the formation of gel-like films caused by decomposition of electrolyte [40]. However, it does not present in all of the carbon/iron oxide anode systems, so the capacity increase should also be related with the interfacial interaction between carbon (or Cu) and iron oxide [42]. It is worth mentioning here that the obtained value of CuO/reduced graphene oxide nanocomposite is still much higher than the theoretical capacity of conventional anode graphite (372 mAh g^{-1}). More importantly, the cycling stability of CuO/reduced graphene oxide nanocomposite electrode is much better than that of pure CuO nanoparticles electrode, indicating that reduced graphene nanosheets can further improve the cycle performance of CuO owing to its high electrical conductivity and good buffer role. In addition, the strong interfacial interaction in nanocomposite possibly promotes the quick transfer of electron between reduced graphene nanosheets and CuO to some extent, and leads to the slight increase of specific capacity with cycles.

To examine the effectiveness of reduced graphene nanosheets and nanostructures in improving the rate capability of anodes, we investigated the specific capacity of pure CuO nanoparticles and their nanocomposites under various current densities and the result is plotted in Fig. 4. Both the cells were cycled between 0.01 and 3 V under various current densities from 0.1 mA cm^{-2} to 6.4 mA cm^{-2}. Compared to the pure CuO nanoparticles, the specific capacities of CuO/reduced graphene oxide nanocomposite are

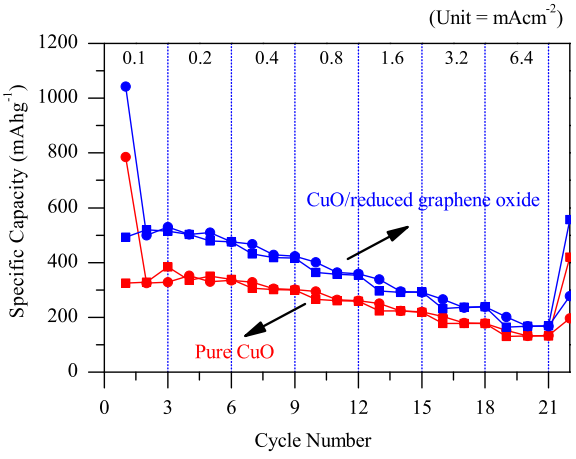

Fig. 4. Comparison of the rate capabilities of the pure CuO nanoparticles and CuO/reduced graphene oxide nanocomposite at various current densities between 0.1 and 6.4 mA cm^{-2}.

substantially increased at all investigated discharge/charge current densities. The nanocomposite electrode delivers an initial discharge capacity of 1043.3 mAh g^{-1} at 0.1 mA cm^{-2}, 503.2 mAh g^{-1} at 0.2 mA cm^{-2}, 466.9 mAh g^{-1} at 0.4 mA cm^{-2}, 401.3 mAh g^{-1} at 0.8 mA cm^{-2}, 338.1 mAh g^{-1} at 1.6 mA cm^{-2}, 265.9 mAh g^{-1} at 3.2 mA cm^{-2} and 201.1 mAh g^{-1} at 6.4 mA cm^{-2}. While the pure exhibit an initial discharge capacity of 785.2 mAh g^{-1}, 352.8 mAh g^{-1}, 327.9 mAh g^{-1}, 293.7 mAh g^{-1}, 251.3 mAh g^{-1}, 203.9 mAh g^{-1} and 152.8 mAh g^{-1} at the same current densities. It can be clearly seen that the capacity of pure CuO nanoparticles has only a slight fading at high current density of 6.4 mA cm^{-2}. It is worth noting that pure CuO nanoparticles electrode obtained in the present study has also potential to produce promising capacities even at high current density also. Additionally, the observed discharge/charge capacity at high current density and cycle number values are comparable than those reported for pure CuO nanoparticles, but the synthesis adopted in the present study is very cost-effective and very simple compared to that in the previously reported counterparts [16,21,43]. Furthermore, the improved rate capacity of CuO/reduced graphene oxide nanocomposite probably originates due to the following factors. The CuO nanoparticles appear to be homogenously anchored on to the reduced graphene oxide nanosheets. Further, the flexible nanosheets facilitate the accommodation of volumetric variations normally observed for CuO during Li-intercalation/de-intercalation. In addition, the presence of reduced graphene oxide nanosheets prevents particle aggregation and evades the problems of electrode pulverization on repeated electrochemical cycling. Moreover, reduced graphene oxide nanosheets serve as good electrical conductors and promote the reduction in internal resistance of the Li-ion batteries which ultimately benefits electrode specific capacities. Since Li-ion diffusion is dependent on the ion-transport length and accessible active material surface sites, the nano-sized CuO particles in combination with the reduced graphene oxide nanosheets may provide shorter ion transport path lengths and enhancements in electrode/electrolyte contact area and thereby lead to higher storage capacities, coulombic efficiencies and cycling stabilities [26]. On the basis of the above analyses, it is concluded that the synergetic effect between conducting reduced graphene oxide nanosheets and CuO nanoparticles is responsible for the excellent electrochemical performance of the overall electrode via the maximum utilization of electrochemically active reduced graphene and nanosized CuO nanoparticles.

To further testify the enhanced electronic conductivity, EIS measurements on pure CuO nanoparticles and their nanocomposite electrodes were performed after 3 charge/discharge cycles as shown in Fig. 5. According to previous reports [44], the intercept impedance on the Z-real axis reflects the electrolyte solution resistance, while the semicircle in the high–middle frequency range and the oblique line at low frequencies represents the charge-transfer process and the lithium ion diffusion process (Warburg), respectively. It can be clearly seen that both of the Nyquist plots are composed of two parts, one semicircle and one straight line. The semicircle in the high–middle frequency region is related to charge-transfer process occurring at the electrode/electrolyte interface and the straight line in the low frequency region can be attributed to Warburg impedance. The smaller the charge transfer resistance, the smaller the diameter of the semicircle. The results of the fitting analysis indicate that the charge transfer resistance value of the nanocomposite electrode is 36 Ω, which is much lower than that of the pure nanoparticles electrode (ca. 46.5 Ω), which indicates a smaller charge transfer resistance and the greater facilitation of electronic transportation during the electrochemical reactions (details referred to in Ref. [45]). However, the results suggest that the highly conductive

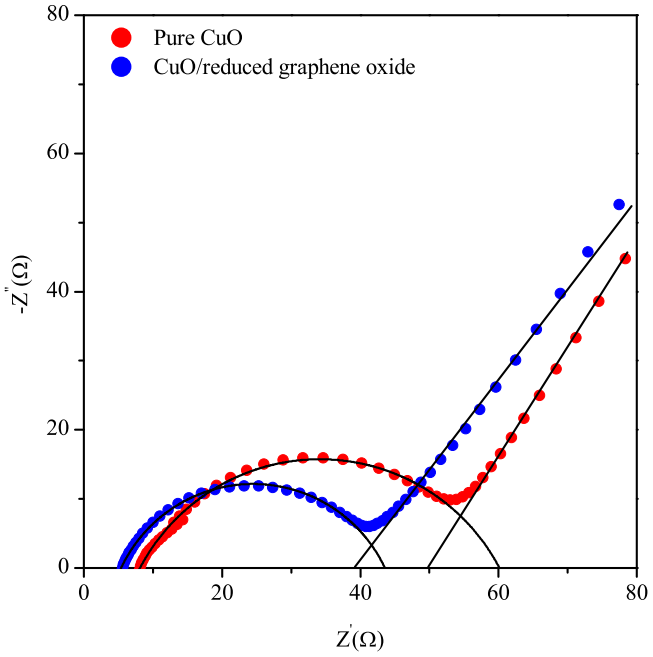

Fig. 5. Nyquist plots of pure CuO nanoparticles and CuO/reduced graphene oxide nanocomposite electrodes measured in the frequency range between 0.01 Hz and 1.0 MHz.

reduced graphene nanosheets can facilitate electron transfer and thus decreasing resistance. Therefore, improved high rate performance and the depressed polarization could be attributed to the substantial decrease in charge-transfer resistance.

4. Conclusions

In summary, first, pure CuO nanoparticles were successfully synthesized by simple, straightforward and inexpensive microwave-assisted synthesis method within a fast reaction time of less than 20 min, followed by calcination at 500 °C for 5 h. Further, the CuO/reduced graphene oxide nanocomposite was successfully synthesized by milling of a mixture of obtained pure CuO nanoparticles and 10 wt% of reduced graphene nanosheets using high energy spex mill for 1 min. By short-time spex-milling, a unique CuO/reduced graphene oxide nanocomposite is obtained with a microstructure of multi-scale CuO nanoparticles homogeneously dispersed in a reduced graphene matrix. The synthesized products were characterized using XRD, FE-TEM and HR-TEM techniques. The particle size was found in the range of 60–65 nm and 40–65 nm with an irregular shaped morphology for pure CuO nanoparticles and their nanocomposite respectively. When tested for lithium storage, the CuO/reduced graphene oxide nanocomposite anode demonstrated significantly improved cycling performance compared to the pure CuO nanoparticles. Based on the electrochemical studies, the initial discharge capacity of the pure CuO nanoparticles and CuO/reduced graphene oxide nanocomposite are 785.2 mAh g^{-1} and 1043.3 mAh g^{-1} respectively. Moreover, the nanocomposite exhibited a second reversible discharge capacity of 496.5 mAh g^{-1} at 0.1 mA cm^{-2} and more importantly, could retain almost 96% of coulombic efficiency without obvious capacity fading over 45 cycles (516.4 mAh g^{-1}), demonstrating excellent capacity retention of the electrode. After 45 cycles, the capacity attained for the nanocomposite is 32% higher than that observed for pure CuO nanoparticles (392.1 mAh g^{-1}). Even at a high current density of 6.4 mA cm^{-2}, the reversible capacity of nanocomposite is still as high as 201.1 mAh g^{-1}, which is higher than that of the pure CuO

nanoparticles (152.8 mAh g^{-1}). The excellent electrochemical performance of the nanocomposite can be attributed to that reduced graphene served as dispersing medium to prevent CuO nanoparticles from agglomeration, alleviating the pulverization and provide an excellent electronic conduction pathway. Moreover, our simple synthesis method can be readily adapted to prepare other composites in which reduced graphene nanosheets not only acts as a conducting additive to support metal oxide nanoparticles, but also provides additional electrochemical active sites to further enhance their electrochemical performance.

Acknowledgments

This work was supported by Priority Research Centers Program through the National Research Foundation of Korea (NRF) funded by the Ministry of Education, Science and Technology (2009-0094055). This research was also supported by the MKE (The Ministry of Knowledge Economy), Korea, under the ITRC (Information Technology Research Center) support program supervised by the NIPA (National IT Industry Promotion Agency) (NIPA-2012-H0301-12-1009).

References

[1] K.S. Kang, Y.S. Meng, J. Breger, C.P. Grey, G. Ceder, Science 311 (2006) 977–980.
[2] C.K. Chan, H.L. Peng, G. Liu, K. McIlwrath, X.F. Zhang, R.A. Huggins, Y. Cui, Nat. Nanotechnol. 3 (2008) 31–35.
[3] B. Kang, G. Ceder, Nature 458 (2009) 190–193.
[4] D. Liu, G. Cao, Energy Environ. Sci. 3 (2010) 1218–1237.
[5] H. Buqa, D. Goers, M. Holzapfel, M.E. Spahr, P. Novak, J. Electrochem. Soc. 152 (2005) A474–A481.
[6] F.L. Cheng, J. Liang, Z.L. Tao, J. Chen, Adv. Mater. 23 (2011) 1695–1715.
[7] M.G. Kim, J. Cho, Adv. Funct. Mater. 19 (2009) 1497–1514.
[8] Y. Xie, C.Z. Wu, Dalton Trans. (2007) 5235–5240.
[9] L.Q. Lu, Y. Wang, J. Mater. Chem. 21 (2011) 17916–17921.
[10] L. Aldon, J.-C. Jumas, Solid State Sci. 14 (2012) 354–361.
[11] C.M. Ionica-Bousquet, P.E. Lippens, L. Aldon, J. Olivier-Fourcade, J.C. Jumas, Chem. Mater. 18 (2006) 6442–6447.
[12] P. Poizot, S. Laruelle, S. Grugeon, L. Dupont, J.M. Tarascon, Nature 407 (2000) 496–499.
[13] J. Zhang, J. Liu, Q. Peng, X. wang, Y. Li, Chem. Mater. 18 (2006) 867–871.
[14] Y. Chang, J.J. Teo, H.C. Zeng, Langmuir 21 (2005) 1074–1079.
[15] J.C. Park, J. Kim, H. Kwon, H. Song, Adv. Mater. 21 (2009) 803–807.
[16] Y.J. Mai, X.L. Wang, J.Y. Xiang, Y.Q. Qiao, D. Zhang, C.D. Gu, J.P. Tu, Electrochim. Acta 56 (2011) 2306–2311.
[17] S.Q. Wang, J.Y. Zhang, C.H. Chen, Scr. Mater. 57 (2007) 337–340.
[18] F.S. Ke, L. Huang, G.Z. Wei, L.J. Xue, J.T. Li, B. Zhang, S.R. Chen, X.Y. Fan, S.G. Sun, Electrochim. Acta 54 (2009) 5825–5829.
[19] J.Y. Xiang, J.P. Tu, L. Zhang, Y. Zhou, X.L. Wang, S.J. Shi, J. Power Sources 195 (2010) 313–319.
[20] L.J. Fu, J. Gao, T. Zhang, Q. Cao, L.C. Yang, Y.P. Wu, R. Holze, H.Q. Wu, J. Power Sources 174 (2007) 1197–1200.
[21] X.H. Huang, C.B. Wang, S.Y. Zhang, F. Zhou, Electrochim. Acta 56 (2011) 6752–6756.
[22] M.D. Stoller, S. Park, Y. Zhu, J. An, R.S. Ruoff, Nano Lett. 8 (2008) 3498–3502.
[23] K.I. Bolotin, K.J. Sikes, Z. Jiang, M. Klima, G. Fudenberg, J. Hone, P. Kim, H.L. Stormer, Solid State Commun. 146 (2008) 351–355.
[24] C. Lee, X. Wei, J.W. Kysar, J. Hone, Science 321 (2008) 385–388.
[25] G.M. Zhou, D.W. Wang, F. Li, L.L. Zhang, N. Li, Z.S. Wu, L. Wen, G.Q. Lu, H.M. Cheng, Chem. Mater. 22 (2010) 5306–5313.
[26] Z.S. Wu, W.C. Ren, L. Wen, L.B. Gao, J.P. Zhao, Z.P. Chen, G.M. Zhou, F. Li, H.M. Cheng, ACS Nano 4 (2010) 3187–3194.
[27] L. Taoa, J. Zaia, K. Wanga, H. Zhanga, M. Xua, J. Shena, Y. Sub, X. Qiana, J. Power Sources 202 (2012) 230–235.
[28] G. Wang, J. Liu, S. Tang, H. Li, D. Cao, J. Solid State Electrochem. 15 (2011) 2587–2592.
[29] B. Wang, Y. Wang, J. Park, H. Ahn, G. Wang, J. Alloys Compd. 509 (2011) 7778–7783.
[30] P. Lian, X. Zhu, H. Xiang, Z. Li, W. Yang, H. Wang, Electrochim. Acta 56 (2010) 834–840.
[31] S. Liang, X. Zhu, P. Lian, W. Yang, H. Wang, J. Solid State Chem. 184 (2011) 1400–1404.
[32] Y. Shi, L. Wen, F. Li, H.-M. Cheng, J. Power Sources 196 (2011) 8610–8617.
[33] W.S. Hummers, R.E. Offeman, J. Am. Chem. Soc. 80 (1958). 1339–1339.
[34] A.K. Rai, J. Gim, J. Song, V. Mathew, L.T. Anh, J. Kim, Electrochim. Acta 75 (2012) 247–253.
[35] P. Lian, X. Zhu, S. Liang, Z. Li, W. Yang, H. Wang, Electrochim. Acta 56 (2011) 4532–4539.
[36] M. Wan, D. Jin, R. Feng, L. Si, M. Gao, L. Yue, Inorg. Chem. Commun. 14 (2011) 38–41.
[37] J. Maier, Nat. Mater. 4 (2005) 805–815.
[38] G. Gachot, S. Grugeon, M. Armand, S. Pilard, P. Guenot, J.M. Tarascon, S. Laruelle, J. Power Sources 178 (2008) 409–421.
[39] B. Wang, X.L. Wu, C.Y. Shu, Y.G. Guo, C.R. Wang, J. Mater. Chem. 20 (2010) 10661–10664.
[40] (a) L. Wang, Y. Yu, P.C. Chen, D.W. Zhang, C.H. Chen, J. Power Sources 183 (2008) 717–723;
(b) P. Adelhelm, Y.S. Hu, M. Antonietti, J. Maier, B.M. Smarsly, J. Mater. Chem. 19 (2009) 1616–1620.
[41] P.L. Taberna, S. Mitra, P. Poizot, P. Simon, J.M. Tarascon, Nat. Mater. 5 (2006) 567–573.
[42] J. Zhou, H. Song, L. Ma, X. Chen, RSC Adv. 1 (2011) 782–791.
[43] Y. Hu, X. Huang, K. Wang, J. Liu, J. Jiang, R. Ding, X. Ji, X. Li, J. Solid State Chem. 183 (2010) 662–667.
[44] S. Yang, H. Song, X. Chen, Electrochem. Commun. 8 (2006) 137–142.
[45] M.S. Park, Y.M. Kang, G.X. Wang, S.X. Dou, H.K. Liu, Adv. Funct. Mater. 18 (2008) 455–461.